Total absorption peak by use of a rigid frame porous layer backed by a rigid multi-irregularities grating

J.-P. Groby[a] and W. Lauriks
Laboratory of Acoustics and Thermal Physics, KULeuven, B-3001 Heverlee, Belgium

T. E. Vigran
Acoustics, Department of Electronics and Telecommunications, Norwegian University of Science and Technology (NTNU), NO-7491 Trondheim, Norway

(Received 24 March 2009; revised 1 February 2010; accepted 7 February 2010)

The acoustic properties of a low resistivity porous layer backed by a rigid plate containing periodic rectangular irregularities, creating a multicomponent diffraction gratings, are investigated. Numerical and experimental results show that the structure possesses a total absorption peak at the frequency of the modified mode of the layer, when designed as proposed in the article. These results are explained by an analysis of the acoustic response of the whole structure and especially by the modal analysis of the configuration. When more than one irregularity per spatial period is considered, additional higher frequency peaks are observed.
 [DOI: 10.1121/1.3337235]

PACS number(s): 43.55.Ev, 43.20.Fn, 43.20.Ks, 43.20.Gp [KVH] Pages: 2865–2874

I. INTRODUCTION

This work was initially motivated by a design problem connected to the determination of the optimal profile of discontinuous spatial distribution of porous materials and geometric properties for the absorption of sound. Porous materials (foam) suffer from a lack of absorption at low frequencies, when compared to the values at higher frequencies. The usual way to solve this problem is by multilayering.[1–3] The purpose of the present article is to investigate an alternative to multilayering by considering periodic irregularities of the rigid plate on which a porous sheet is attached, thus creating a diffraction grating.

Acoustic wave propagation in porous materials was mainly studied in order to deal with sound absorption,[4] material properties characterization, etc. Homogeneous porous materials are well described by the first work of Biot[5,6] and later contributions.[7–9] On the other hand, the equation that describes acoustic wave propagation in a macroscopically inhomogeneous rigid frame porous medium was only recently derived in Ref. 10 from the alternative formulation of Biot's theory.[6] The latter approach could eventually offer an alternative to multilayering in the sense that it can be applied to the design of (e.g., functionally gradient) rigid frame media with continuously varying properties.

The influence of the addition of a volumic heterogeneity on absorption and transmission of porous layers was previously investigated by use of the multipole method in Refs. 11 and 12 by embedding a periodic set of high-contrast inclusions, whose size is not small compared with the wavelength, in a macroscopically homogeneous porous layer whose thickness and weight are relatively small. This leads either to an increase in the absorption coefficient in the case of one layer of inclusions or to band gaps and a total absorption peak in case of multilayered inclusions (sonic crystal). The influence on the absorption coefficient was explained by mode excitation of the configuration enabled by the periodic inclusions, whose structure leads to energy entrapment. Other works related to volumic heterogeneities in macroscopically homogeneous porous material were carried out essentially by means of the homogenization procedure.[13–15]

Periodic arrangements of either surface irregularities or volume heterogeneities usually lead to energy entrapment either at the surface or inside the structure, this being strongly linked to mode excitation and to an increase in the absorption coefficient (first noticed by Wood[16] and partially explained by Cutler[17]). The particular properties of such structures have been studied in mechanics, with application to composite materials, in optics initially motivated by the collection of solar energy[18,19] with applications to photonic crystals,[20,21] in electromagnetics with application to so-called left-handed materials,[22] and in geophysics for the study of the "city-site" effect.[23–25] Absorption properties of such structures, even involving only one surface irregularity per spatial period, is still a relevant problem in optics.[26] The properties of such structures have been used for the design of sound absorbing properties of porous materials using porous slits or fractals.[11,12,27–29]

Here, we investigate theoretically, numerically, and experimentally the influence on the absorption coefficient of a multicomponent gratings against which a rigid frame porous layer is glued. The modal analysis shows that the modified mode of the layer can easily be excited by use of such periodic arrangement, this being associated with an entrapment of the energy and so a possible large absorption. Numerical experiments allow us to propose a design process for the irregularities in order for the configuration to possess a total

[a]Author to whom correspondence should be addressed. Electronic mail: Jean-Philippe.Groby@univ-lemans.fr. Present address: Laboratoire d'Acoustique de l'Université du Maine, UMR6613 CNRS/Univ. du Maine, F-72085 Le Mans Cedex 9, France.

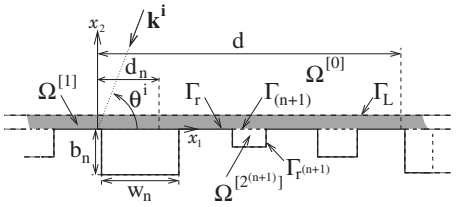

FIG. 1. Cross-sectional plane representation of a d-periodic fluidlike porous plate backed by a rigid wall that contains periodic rectangular and macroscopic irregularities excited by a plane incident wave.

absorption peak at low frequency. Experiments, performed in a square impedance tube, are in agreement with the theoretical and numerical developments.

II. FORMULATION OF THE PROBLEM

A. Description of the configuration

Both the incident plane acoustic wave and the geometrical configuration are assumed to be invariant with respect to the Cartesian coordinate x_3. A cross-sectional x_1-x_2 plane view of the two-dimensional (2D) scattering problem is shown in Fig. 1.

Before the addition of the structured backing, the layer is a porous material saturated by air (e.g., a foam) which is modeled (by homogenization) as a (macroscopically homogeneous) equivalent fluid $M^{[1]}$. The upper and lower flat and mutually parallel boundaries of the layer, whose x_2 coordinates are L and 0, are designated by Γ_L and Γ_0, respectively. $M^{[0]}$ and $M^{[1]}$ are in firm contact through Γ_L, i.e., the pressure and normal velocity are continuous across Γ_L ($[p(\mathbf{x})]=0$ and $[\rho^{-1}\partial_n p(\mathbf{x})]=0$, wherein ∂_n designates the operator $\partial_n=\mathbf{n}\cdot\nabla$and $\mathbf{n}$ denotes the generic unit vector normal to a boundary). The rigid backing contains N rectangular irregularities along the x_1 axis with period d that create a diffraction grating. The nth irregularity of the unit cell occupies the rectangular domain $\Omega^{[2^{(n)}]}$ of height b_n and width w_n and is occupied by a fluid material $M^{[2]}$ (in this study, $M^{[2]}$ is the air medium, but according to the formulation developed hereafter it can be any other fluidlike material). The boundary of $\Omega^{[2^{(n)}]}$ is composed of the rigid portion $\Gamma_{r^{(n)}}$ [Neumann type boundary conditions, $\partial_n p(\mathbf{x})=0$] and of $\Gamma_{(n)}$ through which media $M^{[2]}$ and $M^{[1]}$ are in firm contact (continuity of the pressure and normal velocity). The x_1 coordinate of the center of the base segment of $\Omega^{[2^{(n)}]}$ is d_n. Γ_0 is also composed of a rigid portion Γ_r (Neumann type boundary conditions).

We denote the total pressure, wavenumber, and wave speed by the generic symbols p, k, and c, respectively, with $p=p^{[0]}$, $k=k^{[0]}=\omega/c^{[0]}$ in $\Omega^{[0]}$, $p=p^{[1]}$, $k=k^{[1]}=\omega/c^{[1]}$ in $\Omega^{[1]}$, and $p=p^{[2^{(n)}]}$, $k=k^{[2]}=\omega/c^{[2]}$ in $\Omega^{[2^{(n)}]}$.

Rather than to solve directly for the pressure $\bar{p}(\mathbf{x},t)$ [with $\mathbf{x}=(x_1,x_2)$], we prefer to deal with $p(\mathbf{x},\omega)$, related to $\bar{p}(\mathbf{x},t)$ by the Fourier transform $\bar{p}(\mathbf{x},t)=\int_{-\infty}^{\infty}p(\mathbf{x},\omega)e^{-i\omega t}d\omega$. Henceforth, we drop the ω in $p(\mathbf{x},\omega)$ so as to denote the latter by $p(\mathbf{x})$.

The wavevector $\mathbf{k}^i$ of the incident plane wave lies in the sagittal plane and the angle of incidence θ^i is measured counterclockwise from the positive x_1 axis. The incident wave propagates in $\Omega^{[0]}$ and is expressed by $p^i(\mathbf{x})=A^i e^{i(k_1^i x_1-k_2^{[0]i}(x_2-L))}$, wherein $k_1^i=-k^{[0]}\cos\theta^i$, $k_2^{[0]i}=k^{[0]}\sin\theta^i$, and $A^i=A^i(\omega)$ is the signal spectrum.

The plane wave nature of the incident wave and the periodic nature of $\cup_{n\in\mathcal{N}}\Omega^{[2^{(n)}]}$ imply the Floquet relation,

$$p(x_1+qd,x_2)=p(x_1,x_2)e^{ik_1^i qd};\quad \forall\,\mathbf{x}\in\mathbb{R}^2;\quad \forall\,q\in\mathbb{Z}. \tag{1}$$

Consequently, it suffices to examine the field in the central cell of the plate which includes the rectangulars $\Omega^{[2^{(n)}]}$, $n\in\mathcal{N}$ in order to obtain the fields, via the Floquet relation, in the other cells.

The uniqueness of the solution to the forward-scattering problem is assured by the radiation condition:

$$p^{[0]}(\mathbf{x})-p^i(\mathbf{x})\sim\text{outgoing waves};\quad |\mathbf{x}|\to\infty,\quad x_2>L. \tag{2}$$

B. Material modeling

Rigid frame porous materials M are modeled using the Johnson–Champoux–Allard model. The compressibility and density of these media, linked to the sound speed through $c=\sqrt{1/(K\rho)}$, are[9,10]

$$\frac{1}{K}=\frac{\gamma P_0}{\phi\left(\gamma-(\gamma-1)\left(1+i\frac{\omega_c}{\mathrm{Pr}\,\omega}G(\mathrm{Pr}\,\omega)\right)^{-1}\right)},$$

$$\rho=\frac{\rho_f\alpha_\infty}{\phi}\left(1+i\frac{\omega_c}{\omega}F(\omega)\right), \tag{3}$$

wherein $\omega_c=\sigma\phi/\rho_f\alpha_\infty$ is the Biot frequency, γ is the specific heat ratio, P_0 is the atmospheric pressure, Pr is the Prandtl number, ρ_f is the density of the fluid in the (interconnected) pores, ϕ is the porosity, α_∞ is the tortuosity, and σ is the flow resistivity. The correction functions $G(\mathrm{Pr}\,\omega)$ (Ref. 30) and $F(\omega)$ (Ref. 7) are given by

$$G(\mathrm{Pr}\,\omega)=\sqrt{1-i\eta\rho_f\,\mathrm{Pr}\,\omega\left(\frac{2\alpha_\infty}{\sigma\phi\Lambda'}\right)^2},$$

$$F(\omega)=\sqrt{1-i\eta\rho_f\omega\left(\frac{2\alpha_\infty}{\sigma\phi\Lambda}\right)^2}. \tag{4}$$

where η is the viscosity of the fluid, Λ' is the thermal characteristic length, and Λ is the viscous characteristic length.

The configuration is more complex than the one already studied (for shear horizontal waves) in Ref. 24 by one of the author of this paper, in the sense that more than one irregularity per spatial period is accounted for. We also briefly summarize the method of solution hereafter.

C. Field representations in $\Omega^{[0]}$, $\Omega^{[1]}$, and $\Omega^{[2^{(n)}]}$

Separation of variables, the radiation condition, and the Floquet theorem lead to the representations:

$$p^{[0]}(\mathbf{x}) = \sum_{q\in\mathbb{Z}} [e^{-ik_{2q}^{[0]}(x_2-L)}\delta_q + R_q e^{ik_{2q}^{[0]}(x_2-L)}] \times e^{ik_{1q}x_1}, \quad \forall\, \mathbf{x} \in \Omega^{[0]},$$

$$p^{[1]}(\mathbf{x}) = \sum_{q\in\mathbb{Z}} [f_p e^{-ik_{2q}^{[1]}x_2} + g_p e^{ik_{2q}^{[1]}x_2}] \times e^{ik_{1q}x_1}, \quad \forall\, \mathbf{x} \in \Omega^{[1]}, \tag{5}$$

wherein δ_q is the Kronecker symbol, $k_{1q}=k_1^i+(2q\pi/d)$, $k_{2q}^{[s]}=\sqrt{(k^{[s]})^2-(k_{1q})^2}$, with $\mathrm{Re}(k_{2q}^{[s]})\geq 0$ and $\mathrm{Im}(k_{2q}^{[s]})\geq 0$, $s=0,1$. R_q is the reflection coefficient of the plane wave denoted by the subscript q, whose angle is $\theta_q=-i\log((k_{1q}+ik_{2q}^{[1]})/k^{[1]})$, while f_q and g_q are the coefficients of the diffracted waves inside the slab associated with the plane wave also denoted by the subscript q.

Referring to Ref. 24, the pressure fields $p^{[2^{(n)}]}$ admits the pseudomodal representation that already accounts for the boundary conditions on $\Gamma_{r^{(n)}}$:

$$p^{[2^{(n)}]}(\mathbf{x}) = \sum_{m=0}^{\infty} B_m^{(n)} \cos(k_{1m}^{[2^{(n)}]}(x_1 - d_n + w_n/2)) \times \cos(k_{2m}^{[2^{(n)}]}(x_2 + b_n)), \quad \forall\, \mathbf{x} \in \Omega^{[2^{(n)}]}, \quad \forall\, n \in \mathcal{N}, \tag{6}$$

wherein $k_{1m}^{[2^{(n)}]}=m\pi/w_n$, $k_{2m}^{[2^{(n)}]}=\sqrt{(k^{[2]})^2-(k_{1m}^{[2^{(n)}]})^2}$, with $\mathrm{Re}(k_{2m}^{[2^{(n)}]})\geq 0$ and $\mathrm{Im}(k_{2m}^{[2^{(n)}]})\geq 0$, $\forall n\in\mathcal{N}$ and $B_m^{(n)}$ are the coefficients of the pseudomodal representation.

III. DETERMINATION OF THE ACOUSTIC PROPERTIES OF THE STRUCTURE

A. Application of the continuity conditions across Γ_L and Γ_0

Applying the continuity of the pressure field and of the normal component of the velocity across Γ_L and Γ_0, introducing the appropriate field representation therein, Eqs. (5) and (6), and making use of the orthogonality relations $\int_{-d/2}^{d/2} e^{i(k_{1q}-k_{1l})x_1}dx_1 = d\delta_{ql}$, $\forall\,(l,n)\in\mathbb{Z}^2$ and $\int_0^{w_n}\cos(k_{1m}^{[2^{(n)}]}x_1)\times\cos(k_{1j}^{[2^{(n)}]}x_1)dx_1 = w_n\delta_{mj}/\epsilon_m$, $\forall(j,m)\in\mathbb{N}^2$, wherein $\epsilon_0=1$ and $\epsilon_m=2$, $\forall m\in\mathbb{N}^\star$, give rise to the linear set of equations. After some algebra and rearrangements, this reduces to a linear system of equations for the solution of $B_m^{(n)}$ which may be written in the matrix form, when denoting by $\mathbf{B}$ the infinite column matrix of components $B_m^{(n)}$

$$(\mathbf{A}-\mathbf{C})\mathbf{B} = \mathbf{F}, \tag{7}$$

where $\mathbf{F}$ is the column matrix of elements $\Sigma_{q\in\mathbb{Z}}F_{ql}^{(t)}$ and $\mathbf{A}$ and $\mathbf{C}$ are two square matrices of elements $A_l^{(t)}\delta_{tn}$, and $\Sigma_{q\in\mathbb{Z}}C_{qjm}^{(t,n)}$, respectively. These elements are as follows:

$$F_{ql}^{(t)} = A^i \frac{2\alpha_q^{[0]}\delta_q}{D_q} I_{ql}^{+(t)} e^{ik_{1q}(d_t-w_t/2)},$$

$$A_l^{(t)} = \frac{1}{\epsilon_l}\cos(k_{2l}^{[2^{(t)}]}b_t),$$

$$C_{qjm}^{(t,n)} = \frac{iw_n\alpha_m^{[2^{(n)}]}(\alpha_q^{[1]}\cos(k_{2q}^{[1]}L) - i\alpha_q^{[0]}\sin(k_{2q}^{[1]}L))}{dD_q\alpha_q^{[1]}} \times \sin(k_{2m}^{[2^{(n)}]}b_n) I_{qm}^{-(n)} I_{qj}^{+(t)} e^{ik_{1q}((d_t-d_n)-(w_t-w_n)/2)},$$

$$D_q = \alpha_q^{[0]}\cos(k_{2q}^{[1]}L) - i\alpha_q^{[1]}\sin(k_{2q}^{[1]}L), \tag{8}$$

where $I_{qm}^{\pm(n)}=\int_0^1 e^{\pm ik_{1q}w_n\chi}\cos(k_{1m}^{[2^{(n)}]}\chi w_n)d\chi$, $\alpha_q^{[s]}=k_{2q}^{[s]}/\rho^{[s]}$, $s=0,1$, and $\alpha_m^{[2^{(n)}]}=k_{2m}^{[2^{(n)}]}/\rho^{[2]}$. The components $F_{ql}^{(t)}$ accounts for the excitation of the irregularity t by a wave that is previously diffracted by the layer, the components $A_l^{(t)}$ and $C_{qjm}^{(t,t)}$ account for the irregularity t while the components of $C_{qjm}^{(t,n)}$, $n\neq t$ accounts for the coupling, between the irregularities t and n, through waves that are traveling inside the porous layer.

B. Evaluation of the fields

Once Eq. (7) is solved for $B_m^{(n)}$, R_q, f_q, and g_q in terms of $B_m^{(n)}$ can be evaluated and, in particular,

$$R_q = \delta_q\frac{\alpha_q^{[0]}\cos(k_{2q}^{[1]}L) + i\alpha_q^{[1]}\sin(k_{2q}^{[1]}L)}{D_q} + \sum_{n\in\mathcal{N}}\sum_{m=0}^{\infty}\frac{iw_n\alpha_m^{[2^{(n)}]}}{dD_q}B_m^{(n)}\sin(k_{2m}^{[2^{(n)}]}b_n)I_{qm}^{-(n)}e^{-ik_{1q}(d_n-w_n/2)}. \tag{9}$$

Introduced in the appropriate field expression, it follows

$$p_R^{[0]}(x) = \sum_{q\in\mathbb{Z}}\sum_{n\in\mathcal{N}}\frac{iw_n e^{-ik_{1q}(d_n-w_n/2)}}{dD_q}\sum_{m=0}^{\infty}B_m^{(n)}\alpha_m^{[2^{(n)}]}\sin(k_{2m}^{[2^{(n)}]}b_n)I_{qm}^{-(n)}e^{ik_{1q}x_1+ik_{2q}^{[0]}(x_2-L)} + A^i\frac{\alpha^{[0]i}\cos(k_2^{[1]i}L)+i\alpha^{[1]i}\sin(k_2^{[1]i}L)}{D^i}e^{ik_1^i x_1+ik_2^{[0]i}(x_2-a)},$$

$$p^{[1]}(x) = \sum_{q\in\mathbb{Z}}\sum_{n\in\mathcal{N}}\frac{iw_n(\alpha_q^{[1]}\cos(k_{2q}^{[1]}(L-x_2)) - i\alpha_q^{[0]}\sin(k_{2q}^{[1]}(L-x_2)))e^{-ik_{1q}(d_n-w_n/2)}}{d\alpha_q^{[1]}D_q}\sum_{m=0}^{\infty}B_m^{(n)}\alpha_m^{[2^{(n)}]}\sin(k_{2m}^{[2^{(n)}]}b_n)I_{qm}^{-(n)}e^{ik_{1q}x_1} + A^i\frac{2\alpha^{[0]i}\cos(k_2^{[1]i}x_2)}{D^i}e^{ik_1^i x_1}, \tag{10}$$

wherein $k_{20}^{[s]}=k_2^{[s]i}$, $\alpha_0^{[s]}=\alpha^{[s]i}$, $s=0,1$, and $D_0=D^i$. The latter fields are expressed as a sum of (i) the field in the absence of the irregularities with (ii) the field due to the irregularities of the multicomponent grating.

C. Evaluation of the reflection and absorption coefficients

In case of an incident plane wave with spectrum A^i, the conservation of energy relation takes the form

$$1=\mathcal{A}+\mathcal{R}, \tag{11}$$

with $\mathcal{R}$ and $\mathcal{A}$ the hemispherical reflection and absorption coefficients, respectively, defined by

$$\mathcal{R}=\sum_{q\in\mathbb{Z}}\frac{\mathrm{Re}(k_{2q}^{[0]})}{k_2^{[0]i}}\frac{|R_q|^2}{|A^i|^2}=\sum_{q=-\tilde{q}_-}^{\tilde{q}_+}\frac{k_{2q}^{[0]}}{k_2^{[0]i}}\frac{|R_q|^2}{|A^i|^2}, \tag{12}$$

where $\tilde{q}_\mp$ are such that $\tilde{q}_\mp<d/2\pi(k^{[0]}\pm k_1^i)<\tilde{q}_\mp+1$ and $\mathcal{A}=\mathcal{A}_D+\mathcal{A}_S$, where

$$\begin{aligned}\mathcal{A}_D=&\frac{1}{dk_2^{[0]i}|A^i|^2}\frac{\rho^{[0]}}{\mathrm{Re}(\rho^{[1]})}\int_{\Omega^{[1]}}\mathrm{Im}((k^{[1]})^2)|p^{[1]}(\mathbf{x})|^2d\bar{\omega}\\&+\frac{1}{dk_2^{[0]i}|A^i|^2}\frac{\rho^{[0]}}{\mathrm{Re}(\rho^{[2]})}\sum_{n\in\mathcal{N}}\int_{\Omega^{[2^{(n)}]}}\mathrm{Im}((k^{[2]})^2)\\&\times|p^{[2^{(n)}]}(\mathbf{x})|^2d\bar{\omega}\end{aligned} \tag{13}$$

corresponds to the inner absorption of the domains $\Omega^{[1]}$ and $\Omega^{[2^{(n)}]}$, $\forall n\in\mathcal{N}$. $d\bar{\omega}$ is the differential element of surface in the cross-sectional plane and

$$\begin{aligned}\mathcal{A}_S=&\frac{1}{dk_2^{[0]i}|A^i|^2}\mathrm{Re}\int_{\Gamma_L}\frac{\rho^{[0]}}{\rho^{[1]}}p^{[1]*}(\mathbf{x})\nu_{01}\\&\cdot\nabla p^{[1]}(\mathbf{x})\frac{\mathrm{Im}(\rho^{[1]})}{\mathrm{Re}(\rho^{[1]})}d\gamma\\&+\frac{1}{dk_2^{[0]i}|A^i|^2}\sum_{n\in\mathcal{N}}\mathrm{Re}\int_{\Gamma_{(n)}}\frac{\rho^{[0]}}{\rho^{[1]}}\left(\frac{\mathrm{Im}(\rho^{[1]})}{\mathrm{Re}(\rho^{[1]})}-\frac{\mathrm{Im}(\rho^{[2]})}{\mathrm{Re}(\rho^{[2]})}\right)\\&\times p^{[1]*}(\mathbf{x})\nu_{12}\cdot\nabla p^{[1]}(\mathbf{x})d\gamma\end{aligned} \tag{14}$$

corresponds to the surface absorption related to interfaces Γ_L and $\Gamma_{(n)}$, $\forall n\in\mathcal{N}$. $d\gamma$ is the differential arc length in the cross-sectional plane, ν_{01} (respectively, ν_{12}) is the outward-pointing unit vector to the boundary Γ_L (respectively, $\Gamma_{(n)}$), and p^* is the complex conjugate of p.

$\mathcal{A}_S$ accounts for the absorption induced by the viscous dissipation at the interfaces. Effectively, it is obvious from Eq. (14) that $\mathcal{A}_S$ does not vanish because of nonvanishing $\mathrm{Im}(\rho^{[s]})$, $s=1,2$, which is a consequence of the modeling of viscous dissipation phenomena.[4]

In our calculations, the irregularities are filled with the air medium. Any absorption phenomenon is associated with this material and thus Eqs. (13) and (14) can be simplified because $\mathrm{Im}(\rho^{[2]})$ vanishes. The second term of Eq. (13) vanishes, while the term in brackets of the second part of Eq. (14) reduces to $(\mathrm{Im}(\rho^{[1]})/\mathrm{Re}(\rho^{[1]}))$. The absorption associated with the material properties reduces to the inner absorption of the domain $\Omega^{[1]}$ and to surface absorption related to the bounds of the porous layer.

Nevertheless, because of the complicated shape of $\Omega^{[1]}$ and $\Omega^{[2^{(n)}]}$, but also of the nonvanishing term $\mathcal{A}_S$, $\mathcal{A}$ will be calculated by $\mathcal{A}=1-\mathcal{R}$.

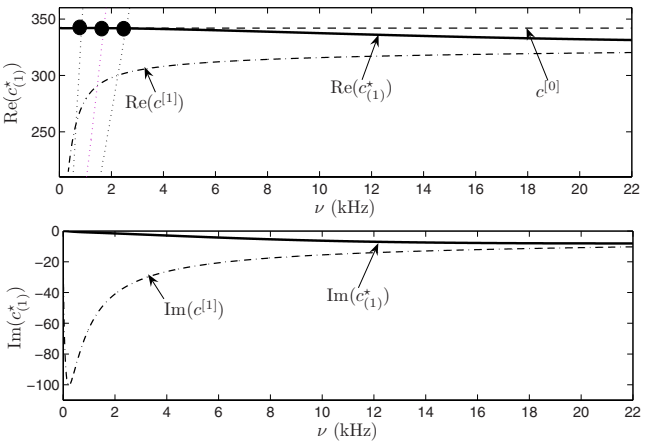

FIG. 2. (Color online) Real and imaginary parts of the root of the dispersion relation in absence of irregularities $c^\star_{(1)}$. Real part of the modified mode of the layer $c^\star_{(1,q)}$, $q=1,\ldots,3$, for $d=40$ cm are pointed out by dot (only the first three modified modes are plotted).

IV. MODAL ANALYSIS OF THE CONFIGURATION

The modes (Pekeris modes in ocean acoustics, quite similar to Love modes for SH polarization in geophysics) of the configuration without irregularities of the rigid backing (i.e., a rigid porous layer backed with a planar rigid wall), whose dispersion relation is

$$D^i=\alpha^{[0]i}\cos(k_2^{[1]i}L)-i\alpha^{[1]i}\sin(k_2^{[1]i}L)=0, \tag{15}$$

cannot be excited by a plane incident wave initially traveling in the air medium.[11,31] Effectively, Fig. 2 depicts the real and the imaginary parts of the roots $c^\star_{(n)}(\omega)=\omega/k^\star_{1,(n)}(\omega)$ of Eq. (15), as calculated with the method already used in Ref. 31 for a $L=0.8$ cm thick porous layer, whose acoustical characteristics are those used in Sec. V. Under the rigid frame assumption and for frequencies higher than the Biot frequency (and lower than the diffusion limit), a porous material can be considered as a modified fluid, its associated dissipation being considered as a perturbation of a fluid. For Eq. (15) to be true without dissipation, $k_2^{[0]}$ should be purely imaginary while $k_2^{[1]}$ should be purely real. Under the previous assumptions, this implies that $\mathrm{Re}(c^\star_{(n)})$ should stand in $[\mathrm{Re}(c^{[1]}),c^{[0]}]$, i.e., $|k_1^i|$ should stand in $[k^{[0]};\mathrm{Re}(k^{[1]})]$. Or for a plane incident wave initially propagating in the air medium $|k_1^i|$ is always smaller than $k^{[0]}$. It is also necessary to note that in the diffusion regime, i.e., for frequencies below the Biot frequency, any mode exists. This fact constitute the major difference when compared with a traditional fluid. Effectively, below the Biot frequency, $k^{[1]}$ is purely imaginary. This implies that $k_2^{[1]}$ is also purely imaginary whatever the value of k_1^i and that D^i never vanishes.

A particular feature of these modes in this configuration is that they are close to $k^{[0]}$ at low frequency, i.e., below 4 kHz.

When the rigid backing presents periodic irregularities, the dispersion relation of the modes of the configuration is $\det(\mathbf{A}-\mathbf{C})=0$. The roots of latter dispersion relation are difficult to determine because of the complex nature of the matrix $\mathbf{A}-\mathbf{C}$.

To get a grip on it, it is convenient to consider one irregularity per spatial period and that a correct representation of the field can be given by accounting only for the fundamental pseudomode (i.e., $m=0$) of the irregularity (i.e., low frequency approximation). The dispersion relation also reduces to

$$1-\sum_{q\in\mathbb{Z}}\frac{iw}{d}\frac{\alpha^{[2]}\tan(k^{[2]}b)\mathrm{sinc}^2\left(k_{1q}\frac{w}{2}\right)}{\alpha_q^{[1]}\frac{\alpha_q^{[0]}\cos(k_{2q}^{[1]}L)-i\alpha_q^{[1]}\sin(k_{2q}^{[1]}L)}{\alpha_q^{[1]}\cos(k_{2q}^{[1]}L)-i\alpha_q^{[0]}\sin(k_{2q}^{[1]}L)}}=0, \quad (16)$$

wherein $\alpha_0^{[2^{(n)}]}=k^{[2]}/\rho^{[2]}=\alpha^{[2]}$.

By referring to Cutler mode,[17] but also to the modal analysis carried out in Ref. 11, the latter dispersion relation is satisfied (in the nondissipative case) when the denominator of Eq. (16) is purely imaginary and vanishes. These conditions are achieved when $|k_{1q}|\in[k^{[0]},\mathrm{Re}(k^{[1]})]$ and when either $D_q=0$ or $\alpha_q^{[1]}=0$ (i.e., $k_{2q}^{[1]}=0$), which, respectively, corresponds to modified modes of the backed-layer (MMBLs) and to modes of the grating (MGs). MMBLs depend on the characteristic of the surrounding material, of the characteristic of the porous layer, on the thickness of the latter, and on the spatial periodicity, while MG only depend on the characteristic of the porous layer and spatial periodicity. Both of them are determined by the intersection of $c_{1q}=\omega/k_{1q}$, respectively, with $\mathrm{Re}(c_{(n)}^{\star}(\omega))$ as calculated for the backed layer and with $\mathrm{Re}(c^{[1]})$. The first three MMBLs are pointed out by the dots on Fig. 2 for porous P1 (see Table II), when the spatial periodicity is $d=40$ cm. The associated attenuation of each mode can then be determined by the values of $\mathrm{Im}(c_{(n)}^{\star})$ and $\mathrm{Im}(c^{[1]})$ at the frequencies at which the modes are excited. The attenuation associated with MG is also higher than the one associated with MMBL for all frequencies. Moreover, MG corresponds to the highest boundary of $|k_{1q}|$ for Eq. (16) to be true. This implies that MG should be difficult to excite. The latter type of mode can only be poorly excited by a plane incident wave, particularly at low frequencies. Phenomenon can be understood as follows because MG corresponds to a configuration with a semi-infinite domain directly above the grating. On one hand, when the thickness of the layer is smaller than or of the same order of the wavelength in the layer, MG can hardly be excited because waves associated with it can hardly stand at the lower bound of the layer, and so modes of the configuration are close to MMBL. On the other hand, when the thickness of the layer is larger than the wavelength in the layer, MG can be excited (if the waves could travel through the layer toward the grating), and so modes of the configuration are close to MG. This latter case corresponds to the asymptotic high-frequency regime of MMBL.

TABLE I. Geometry of the considered configurations, $d=40$ cm and $L=8$ mm.

	N	$d_{n,n+1}$ (cm)	b_n (cm) $\times$ w_n (cm)
C1	1		5×9
C2	2	$d_{12}=8$	$b_1\times w_1=5\times9$ $b_2\times w_2=40\times2$
C3	2	$d_{12}=12$	$b_1\times w_1=5\times9$ $b_2\times w_2=3\times2.5$
C4	4	$d_{12}=12$, $d_{23}=d_{34}=d'=8$	$b_1\times w_1=5\times9$ $b_2\times w_2=1\times2.5$ $b_2\times w_2=b_3\times w_3=b_4\times w_4$

In addition, the approximated dispersion relation, obtained by use of the partition method and studied in Ref. 24, points to the fact that the mode of the global configuration can be understood either as a modified mode of the irregularities (MI) satisfying $\cos(k_{2m}^{[2]^{(n)}}b)=0$ or as a MMBL satisfying $D_q=0$. MI depends on the geometric properties of the irregularities and of the characteristic of the material that fill the latter, i.e., in our case the air medium. Modes of the global configuration are also coupled ones resulting from a complex combination between MI, MMBL, and the MG.

V. NUMERICAL RESULTS, EXPERIMENTAL VALIDATION, AND DISCUSSION

The infinite sum $\Sigma_{q\in\mathbb{Z}}$ over the indices of the k_{1q} is found to depend on the frequency and on the period of the grating. An empirical rule is employed, inspired from Refs. 11 and 12 and determined by performing a large number of numerical experiments $\Sigma_{q=-Q_-}^{Q_+}$ such that $Q_{\mp}=\mathrm{int}(d/2\pi(3\ \mathrm{Re}(k^{[1]})\pm k_1^i))+10$. In the latter equations, $\mathrm{int}(a)$ represents the integer part of a. Considering the foam plate without dissipation, $k_{2q}^{[1]}$ is the last vertical wave number to become purely imaginary when q increases. The previous numerical rule also ensures that the summation is performed at least up to $k_{2q}^{[1]}=i\sqrt{2}|k^{[1]}|$ (nondissipative case) with an added security term equal 10.

In a similar way, the infinite sum $\Sigma_{m=0}^{\infty}$ over the indices of $k_{1m}^{[2[(n)]}$ is truncated $\Sigma_{m=0}^{M_+}$, such that $M_+=\mathrm{int}(3w_n\ \mathrm{Re}(k^{[2^{(n)}]})/\pi)+10$. The previous numerical rule also ensures that the summation is performed at least up to $k_{2m}^{[2^{(n)}]}=i\sqrt{2}|k^{[2^{(n)}]}|$ (nondissipative case) with an added security term equal 10.

Numerical calculations have been performed for various geometrical parameters whose values are reported in Table I, and within the frequency range of audible sound, particularly at low frequencies. The initial configuration C1, which is composed of one irregularity per spatial period, becomes more complex by addition of other irregularities in order to construct configurations C2, C3, and C4. The spatial period is $d=40$ cm. For all calculations, irregularities are filled with air, i.e., the ambient ($M^{[0]}$ and $M^{[2]}$) and saturating fluid is air ($\rho^{[0]}=\rho^{[2]}=\rho_f=1.213$ kg m^{-3}, $c^{[0]}=c^{[2]}=\sqrt{\gamma P_0/\rho_f}$, with

TABLE II. Acoustical parameters of the porous material constituting the layer.

	ϕ	α_∞	Λ (μm)	Λ' (μm)	σ (Nsm^{-4})	$f_c=\omega_c/2\pi$ (Hz)
P1	0.96	1.07	273	672	2843	334

$P_0=1.01325\times10^5$ Pa, $\gamma=1.4$, and $\eta=1.839\times10^{-5}$ kg m^{-1} s^{-1}). One of the main constraints in designing acoustically absorbing materials are the size and weight of the configuration. A $L=8$ mm thick low resistivity foam layer, whose parameters and Biot frequency are reported in Table II, was used. These parameters have been evaluated using the traditional methods described in Ref. 9. In the considered frequency range, the wavelength in the layer is larger than the thickness of the layer. Modes of the configuration should be close to MMBL, while MG should be weakly excited.

The MMBL will be around $\nu_{(1,1)}\approx850$ Hz, $\nu_{(1,2)}\approx1700$ Hz, and $\nu_{(1,3)}\approx2550$ Hz,…, while the MG should be excited around $\nu_1\approx700$ Hz, $\nu_2\approx1500$ Hz, and $\nu_3\approx2300$ Hz.

A. One irregularity per spatial period

Different types of waves correspond to each kind of mode related to the grating (MG and MMBL): evanescent waves in $\Omega^{[1]}$ (and also in $\Omega^{[0]}$) for the MG, and evanescent waves in $\Omega^{[0]}$ and propagative ones in $\Omega^{[1]}$ for the MMBL. In order to determine the type of modes excited by the plane incident wave, we have plotted in Fig. 3 the transfer function as calculated by $\mathrm{TF}=p(\mathbf{x},\omega)/p^{[0]i}(\mathbf{x},\omega)$ on $\Gamma_r(x_2=0)$ at 20 cm from the center of the irregularity $b_1\times w_1=5\times9$ cm^2, when excited at normal incidence. The transfer function is separated on the different intervals corresponding to the different types of waves that are involved in the total pressure calculation: $\mathrm{TF}(\nu)$ is the total transfer function, $\mathrm{TF}_1(\nu)$ is the contribution of the propagative waves in both $\Omega^{[0]}$ and $\Omega^{[1]}$, $\mathrm{TF}_2(\nu)$ is the contribution of the evanescent waves in $\Omega^{[0]}$ and propagative ones in $\Omega^{[1]}$, and $\mathrm{TF}_3(\nu)$ is the contribution of the evanescent waves in both $\Omega^{[0]}$ and $\Omega^{[1]}$. The transfer function possesses a large peak at a low frequency around

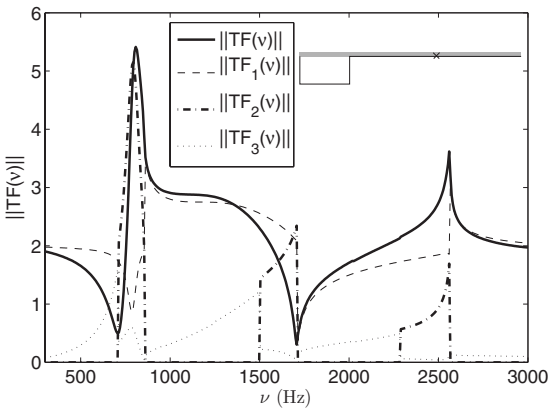

FIG. 3. (Configuration C1) Transfer function on Γ_r at 20 cm from the center of the irregularity, and its different contributions, when the configuration is excited at normal incidence.

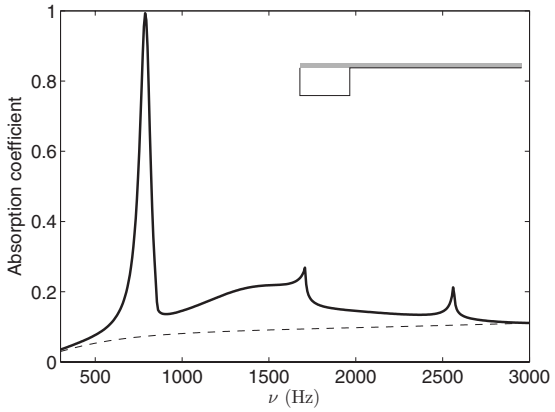

FIG. 4. (Configuration C1) Absorption coefficient for a $L=8$ mm thick foam layer (– – –) backed with a rigid flat plate and (—) backed with a rigid grating $b\times w=5\times9$ cm^2 with $d=40$ cm excited by a normal incident plane wave.

$\nu_{(1,1)}$. The latter is mainly associated with evanescent waves in $\Omega^{[0]}$ and propagative in $\Omega^{[1]}$. This also proves that MMBL are the most excited modes related to the grating, at least at low frequencies. This peak results from a continuous drop between evanescent waves in both material to evanescent waves in the air medium. This also means that this peak is neither a MMBL nor a MG, but result forms a complex combination of these two type of modes, with a structure closer to the one of the MMBL. Because of this structure, the energy is trapped in the layer, this leading to an increase in the absorption of the configuration.

In particular, when the fundamental MI stands at $\nu_{(1,2)}$, i.e., $c^{[2]}/4b_1\approx\nu_{(1,2)}\approx1700$ Hz from which we can determine b_1, and the second MI stands at $\nu_{(1,3)}$, i.e., $c^{[2]}/2\pi\sqrt{(\pi/2b_1)^2+(\pi/w_1)^2}\approx\nu_{(1,3)}\approx2550$ Hz from which we can determine w_1, the absorption at the frequency of the first MMBL is close to 1 (Fig. 4).

This specific feature can be partly explained by the fact that for $\nu_{(1,2)}$ and $\nu_{(1,3)}$, the pressure at $\Gamma_{(1)}$ vanish. The associated waves with both the second and the third modified mode of the backed layer are also unable to correctly stand in the layer, and the energy is also much more trapped by the first MMBL.

Despite the fact that several couples of $b_1\times w_1$ can lead to a total absorption peak, the previously explained rule for the determination of b_1 and w_1 always leads to a total absorption at $\nu_{(1,1)}$ for any value of frequency $\nu_{(1,1)}$ and so for any value of the spatial period d.

When the configuration is designed as proposed, a total absorption peak is also obtained for low resistive porous foam at a frequency which is half of the frequency of the fundamental MI, which allow a reduction in the size of the configuration. The resistivity has a significant influence on the design of such configuration because the frequency of the induced absorption peak should be larger than the Biot frequency $f_c=\omega_c=\sigma\phi/2\pi\rho_f\alpha_\infty$, which greatly depends on the flow resistivity. Effectively, below the Biot frequency, any mode related to the grating can be excited (Sec. IV), and particularly any MMBL exists. In addition, flow resistivity should have an influence on the height of the absorption peak

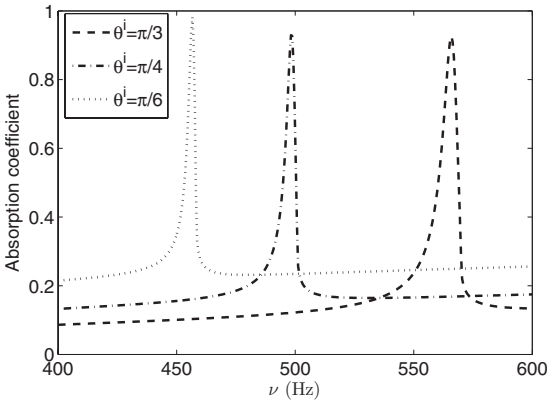

FIG. 5. (Configuration C1) Variation of the absorption peak for a $L=8$ mm thick foam layer backed with a rigid grating $b\times w=5\times 9$ cm^2 with $d=40$ cm as function of the angle of the incident plane wave θ^i.

associated with the first MMBL ($\nu_{(1,1)}\approx 850$ Hz). Effectively, waves associated with the latter mode propagate inside the porous layer. The less resistive the porous material is, the easier these waves can propagate inside the layer. The mode is more easily excited and the absorption is higher at this frequency. In fact, the larger the resistivity is, the more attenuated the first MMBL should be.

Decreasing the angle of incidence leads to a decrease in the frequency of the first MMBL. Effectively, the lower θ^i is, the higher the slope of $c_{1p}=\omega/k_{1p}=\omega/(k^{[0]}\cos(\theta^i)+2p\pi/d)$ is. Figure 5 shows how the absorption peak varies as a function of the angle of incidence. The absorption value of this peak is always higher than 0.9, while the level of the absorption on both sides of the peak is higher if the angle of incidence is smaller (because the incident wave travel much more inside the porous layer).

B. Experimental validation in case of one irregularity per spatial period

Remarkable absorption is obtained in case of periodic irregular rigid backing, while the response of the structure without irregularities is quite well known or at least much more common. Experimental validation also focused on the periodic structure, its effect having been emphasized by comparison with the flat rigid backing in Sec. V A.

Usually, experiments related to 1D or 2D gratings are carried out in a free field (anechoic room) and/or at higher frequencies for a finite size sample.[32]

Here, experimental validation were carried out by use of an impedance tube with a square cross section, 20×20 cm^2, whose cutoff frequency is 850 Hz. The latter corresponds to a wavelength of 40 cm.

The phenomena related to the MMBL occur when the wavelength is of the order of the spatial period of the grating. We also make use of the boundary conditions of the impedance tube, which are perfect mirrors, in order to design the sample. Because of the dimension of the impedance tube, the spatial periodicity should be a multiple of 20 cm. If the profile of the unit cell is symmetric with regard to the axis x_2

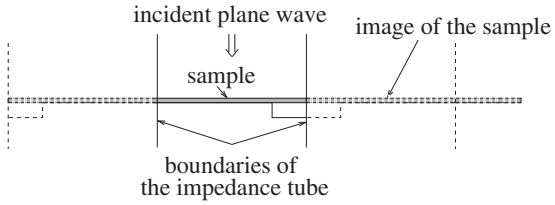

FIG. 6. Cross-sectional view of the experimental setup and sample design.

$=d/2$, the modeled spatial period is $d=40$ cm, as depicted in Fig. 6. Along the x_3 axis, the same idea is employed with use of the image theory.

The infinitely rigid portion of the sample was made of three 1 cm thick aluminum plates, which were screwed (head screw was then filled with hard plastic silicone for the surface to be perfectly flat) in order to create a step of 5 cm height and 4.5 cm width. A $L=8$ mm thick porous foam layer, whose characteristics are those reported in Table II, was glued to the upper part of the step. In order to keep the porous layer flat along the step area, two screws of small diameter (3 mm) were added at both edges of the lower part of the step and a nylon wire was tightened in between, such that the free part of the foam layer rests on it.

The atmospheric pressure were measured at $P_0=997$ kPa. The measured and calculated modes associated with the porous layer also stand at lower frequencies than those calculated in Sec. IV for $P_0=1.013\,25\times 10^5$ Pa. A comparison between the absorption coefficient as measured experimentally and as calculated with the help of the previously presented method is plotted in Fig. 7. The experimental absorption coefficient presents a small and smooth peak at 650 Hz and a total absorption peak at 750 Hz. The first peak is attributed to the fundamental MG because it is weakly excited and occurs at a frequency lower than the other one, while the total absorption peak is attributed to the fundamental MMBL. A first remark is that the total absorption peak lies 40 Hz below its theoretical frequency. This shift can be partly attributed to the fact that the sample is not perfectly perpendicularly mounted in the impedance tube, which leads not only to a small modification of the angle of incidence but also to a modification of the spatial periodicity of the sample due to the mirror effects induced by the boundary conditions.

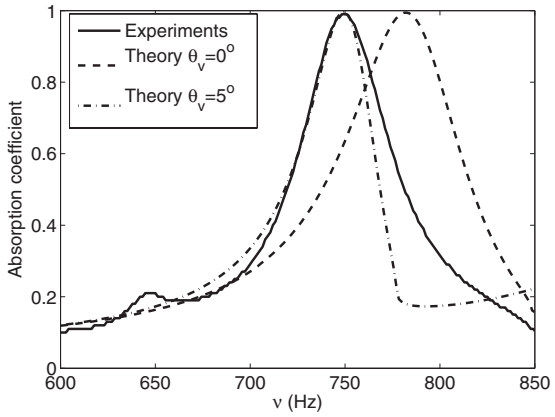

FIG. 7. (Configuration C1) Absorption coefficients as measured experimentally (—), as calculated for $\theta_v=0°$ (– – –) and as calculated for $\theta_v=5°$ (–·–).

Let us consider that the sample is misplaced of an angle θ_v with regard to the cross section of the impedance tube. The angle of incidence and the spatial periodicity become, respectively, $\theta_v^i = \theta^i \pm \theta_v$ and $d_v = d/\cos\theta_v$. When the perturbation θ_v is 5°, the theoretical and experimental total absorption peaks occur at the same frequency, as shown in Fig. 6. Another possible explanation of this frequency shift lies in the experimental boundary conditions itself which are not perfect mirrors, this being hardened by the contacts between the sample and the boundaries which are also not perfect. The fact that the frequency of the total absorption peak is close to the cutoff frequency of the impedance tube, i.e., 850 Hz, is another possible explanation of this frequency shift. A second remark is that the first smooth and small peak attributed to the fundamental MG is not accounted for by the theory. Increasing the number of plane waves involved in the calculation do not induce such a peak. This suggests also some discrepancies between the modeling of the experiments and the experiments itself.

C. Two or more irregularity per spatial period

As pointed out in the modal analysis, the determination of the modes of the global configuration is even more difficult to carry out in case of multiple irregularities per spatial period.

The dimension of the first irregularity is kept as $b_1 \times w_1 = 5 \times 9$ cm^2. Additional irregularities are then added in such a way that the spatial periodicity of the global configuration is constant equal to $d = 40$ cm.

The addition of a second irregularity, whose fundamental resonance frequency is lower than the fundamental MMBL frequency ($\nu_{(1,1)} \approx 850$ Hz), leads to another total absorption peak at the frequency of the fundamental MI, see Fig. 8(a) for $b_2 \times w_2 = 40 \times 2$ cm^2 (frequency of the fundamental MI is ≈400 Hz) and $d_{1,2} = 8$ cm, depending on the center-to-center distance. The fundamental frequency of the corresponding Helmholtz resonator, which satisfies $\sin(k^{[2]}b) = 0$, i.e., $\nu_H = c^{[2]}/2b$, is twice the one of the fundamental MI (which satisfies $c^{[2]}/4b$, Secs. IV and V A). This means that for a fixed dimension of the highest irregularity, the entrapment of energy associated with its resonance in such a configuration appears at a frequency that is half the one of the corresponding Helmholtz resonator. In other words, this means that for a fixed frequency of the associated absorption peak, the height of the irregularity is half the one of a Helmholtz resonator. Such a configuration could also offer a good alternative to the use of Helmholtz resonator, which is the usual way to entrap energy. This result should be temperated by the fact that no thermal and viscous losses are accounted for on the boundaries of the irregularities. Nevertheless, this phenomenon is well known in building engineering or marine architecture, for which the structure is designed for its fundamental frequency to be higher than the one of the ground or of the sea. On the other hand, addition of a smaller size irregularity mainly leads to higher frequency and/or higher amplitude peak either of high order MMBL or of MI, see Fig. 8(b) for $b_2 \times w_2 = 3$ cm $\times 2.5$ cm (frequency of the fundamental MI is ≈2000 Hz) and $d_{1,2} = 12$ cm. This phenomenon was already encountered and studied in the nonperiodic case involving two irregularities.[24] It was attributed to a coupling effect between the irregularities and between the irregularities and the substructure. This coupling leads to a modification of the nature of these types of modes which become coupled ones associated with a higher energy entrapment.

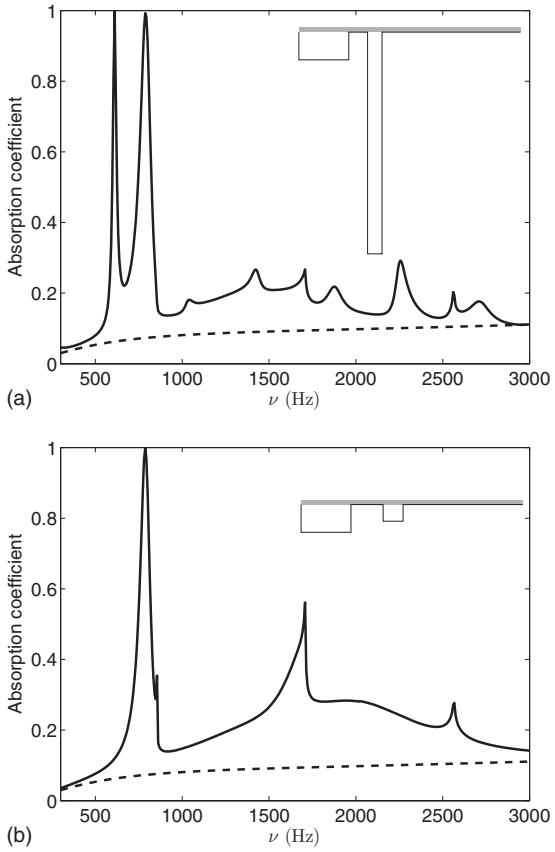

FIG. 8. (Configurations C2 and C3) Absorption coefficient of the foam layer (– – –) backed with a rigid flat plate and (—) backed with two irregularities per spatial period rigid grating, such that $b_1 \times w_1 = 5 \times 9$ cm^2, (a) $b_2 \times w_2 = 40 \times 2$ cm^2 and $d_{1,2} = 8$ cm, and (b) $b_2 \times w_2 = 3 \times 2.5$ cm^2 and $d_{1,2} = 12$ cm.

Adding periodically spaced identical irregularities of smaller size than the irregularity denoted by 1 (the frequency of the fundamental MI is also higher than the one of the fundamental MMBL) leads to a higher frequency peak of absorption associated with the excitation of the corresponding quasi-MMBL, depending on the geometrical characteristics of the irregularities. Effectively, when $d_{i,i+1} = d'$, $i \geq 2$, the quasispatial periodicity d' cannot lead to a total absorption peak because the associated mode is not fully excited, the spatial periodicity of the configuration being d and not d'. This peak can be either interpreted as scattering phenomena occurring over the spatial period d or as a degenerated MMBL associated with d'. Figure 9 shows the absorption coefficient when three identical irregularities $b' \times w' = 1 \times 2.5$ cm^2 equally spaced with $d' = 8$ cm are added, such that $d_{1,2} = 12$ cm. The geometrical dimensions of these irregularities are designed by use of the method presented in Sec. V B. The frequency of the fundamental quasi-MMBL

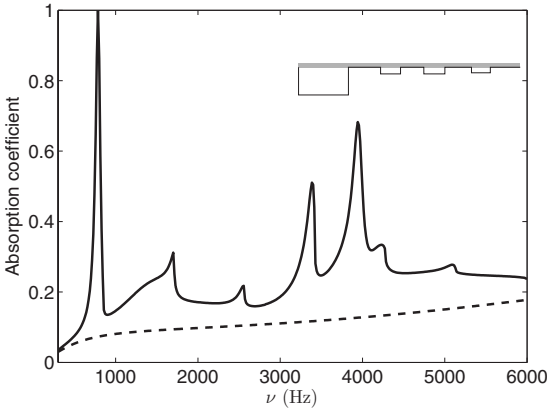

FIG. 9. (Configuration C4) Absorption coefficient of the foam layer (– – –) backed with a rigid flat plate and (—) backed with four irregularities per spatial period rigid grating, such that $b_1 \times w_1 = 5 \times 9$ cm^2 and $b' \times w' = 1 \times 2.5$ cm^2, with $d' = 8$ cm and $d_{1,2} = 12$ cm.

appears at $\nu'_{(1,1)} \approx 4000$ Hz, b' is determined by matching $\nu'_{(1,2)} \approx 8000$ Hz with the fundamental MI, and w' is determined by matching $\nu'_{(1,3)} \approx 12000$ Hz with the second MI.

VI. CONCLUSION

We studied theoretically, numerically, and experimentally the acoustic properties of a low resistivity porous layer backed by a rigid plate with periodic irregularities in the form of a grating.

We show, especially through a modal analysis carried out in the case of only one irregularity per spatial period, that the gratings lead to excitation of modes, whose frequency depends both on the characteristic of the surrounding medium and of the characteristics of the porous layer and on the spatial period of the configuration d. These modes, whose structures are close to the one of the modes of the layer, can lead to a total absorption peak. According to the method proposed to design the irregularity and the configuration, this absorption peak occurs at the frequency of the fundamental modified mode of the layer and seems to be always a total absorption peak when the latter is half of the value of the fundamental frequency of the mode of the irregularity.

Experiments were performed in an impedance tube with square cross section. The boundary conditions of the latter are perfect mirrors and allow us, thanks to the image theory, to model diffraction of a plane wave at normal incidence at frequencies below the cutoff of the tube. Experimental results are in accordance with the theory and particularly exhibit a total absorption peak at the frequency of the fundamental modified mode of the layer.

Addition of more irregularities per spatial period leads to a modification of the modes of the configuration, which becomes coupled and so are associated with a larger entrapment of the energy than the one encountered in the case of only one irregularity. When the fundamental frequency of the irregularity is lower than the fundamental frequency of the modified mode of the layer (i.e., large high irregularity), a total absorption peak is obtained for the fundamental frequency of the irregularity. When the added irregularities are arranged periodically, creating a pseudoperiodicity which leads to pseudomode of the layer (associated with this pseudoperiodicity), a second absorption peak can be created (associated with this pseudoperiodicity), when the irregularities are correctly designed.

[1] L. Brekovskikh, *Waves in Layered Media* (Academic, New York, 1960).
[2] U. Ingard, *Notes on Sound Absorption Technology* (Noise Control Foundation, Poughkeepsie, 1994).
[3] O. Tanneau, J. Casimir, and P. Lamary, "Optimization of multilayered panels with poroelastic components for an acoustical transmission objective," J. Acoust. Soc. Am. **120**, 1227–1238 (2006).
[4] C. Zwicker and C. Kosten, *Sound Absorbing Materials* (Elsevier, Amsterdam, 1949).
[5] M. Biot, "Theory of propagation of elastic waves in fluid-saturated porous solid," J. Acoust. Soc. Am. **28**, 168–178 (1956).
[6] M. Biot, "Mechanics of deformation and acoustic propagation in porous media," J. Appl. Phys. **33**, 1482–1498 (1962).
[7] D. Johnson, J. Koplik, and R. Dashen, "Theory of dynamic permeability and tortuosity in fluid-saturated porous media," J. Fluid Mech. **176**, 379–402 (1987).
[8] K. Attenborough, "Acoustical characteristics of porous materials," Phys. Rep. **82**, 179–227 (1982).
[9] J.-F. Allard, *Propagation of Sound in Porous Media: Modelling Sound Absorbing Materials* (Chapman and Hall, London, 1993).
[10] L. De Ryck, J.-P. Groby, P. Leclaire, W. Lauriks, A. Wirgin, C. Depollier, and Z. Fellah, "Acoustic wave propagation in a macroscopically inhomogeneous porous medium saturated by a fluid," Appl. Phys. Lett. **90**, 181901 (2007).
[11] J.-P. Groby, E. Ogam, and A. Wirgin, "Acoustic response of a periodic distribution of macroscopic inclusions within a rigid frame porous plate," Waves Random and Complex **18**, 409–433 (2008).
[12] J.-P. Groby, A. Wirgin, L. De Ryck, W. Lauriks, R. Gilbert, and Y. Xu, "Acoustic response of a rigid frame porous medium plate with a periodic set of inclusions," J. Acoust. Soc. Am. **126**, 685–693 (2009).
[13] X. Olny and C. Boutin, "Acoustic wave propagation in double porosity media," J. Acoust. Soc. Am. **114**, 73–89 (2003).
[14] C. Boutin, P. Royer, and J.-L. Auriault, "Acoustic absorption of porous surfacing with dual porosity," Int. J. Solids Struct. **35**, 4709–4737 (1998).
[15] V. Tournat, V. Pagneux, D. Lafarge, and L. Jaouen, "Multiple scattering of acoustic waves and porous absorbing media," Phys. Rev. E **70**, 026609 (2004).
[16] R. Wood, "A suspected case of the electrical resonance of minute metal particles for light-waves. A new type of absorption," Proc. Phys. Soc. London **18**, 166–182 (1902).
[17] C. Cutler, "Electromagnetic waves guided by corrugated structures," Technical Report No. MM 44-160-218, Bell Telephone Lab, 1944.
[18] J. Cuomo, J. Ziegler, and J. Woodhall, "A new concept for solar energy thermal conversion," Appl. Phys. Lett. **26**, 557–559 (1975).
[19] C. Horwitz, "Solar-selective globular metal films," J. Opt. Soc. Am. **68**, 1032–1038 (1978).
[20] J. Joannopoulos, R. Meade, and J. Winn, *Photonic Crystals: Molding the Flow of Light* (Princeton University Press, Princeton, 1995).
[21] E. Yablonovitch, "Photonic band-gap structures," J. Opt. Soc. Am. B **10**, 283–295 (1993).
[22] V. Veselago, "The electrodynamics of substances with simultaneous negative value of e and m," Sov. Phys. Usp. **10**, 509–514 (1968).
[23] P.-Y. Bard and A. Wirgin, "Effects of buildings on the duration and amplitude of ground motion in Mexico City," Bull. Seismol. Soc. Am. **86**, 914–920 (1996).
[24] J.-P. Groby and A. Wirgin, "Seismic motion in urban sites consisting of blocks in welded contact with a soft layer overlying a hard half space," Geophys. J. Int. **172**, 725–758 (2008).
[25] C. Boutin and P. Roussillon, "Wave propagation in presence of oscillators on the free surface," Int. J. Eng. Sci. **44**, 180–204 (2006).
[26] N. Bonod, T. Tayeb, D. Maystre, S. Enoch, and E. Popov, "Total absorption of light by lamellar metallic gratings," Opt. Express **16**, 15431–15438 (2008).
[27] A. de Bruijn, "Anomalous effects in the sound absorption of periodically uneven surfaces," Acustica **24**, 75–84 (1971).
[28] L. Kelders, J.-F. Allard, and W. Lauriks, "Ultrasonic surface waves above rectangular-groove gratings," J. Acoust. Soc. Am. **103**, 2730–2733 (1998).
[29] B. Hebert, B. Sapoval, and S. Russ, "Experimental study of a fractal acoustical cavity," J. Acoust. Soc. Am. **105**, 1567–1574 (1999).

[30]J.-F. Allard and Y. Champoux, "New empirical equations for sound propagation in rigid frame porous materials," J. Acoust. Soc. Am. **91**, 3346–3353 (1992).
[31]J.-P. Groby and A. Wirgin, "2D ground motion at a soft viscoelastic layer/hard substratum site in response to SH cylindrical waves radiated by deep and shallow line sources: Numerical results," Geophys. J. Int. **163**, 192–224 (2005).
[32]O. Umnova, K. Attenborough, and C. Linton, "Effects of porous covering on sound attenuation by periodic arrays of cylinders," J. Acoust. Soc. Am. **119**, 278–284 (2006).